Anharmonic IR and Raman spectra and electronic and vibrational (hyper)polarizabilities of barbituric, 2-thiobarbituric and 2-selenobarbituric acids

ARTICLE *in* SPECTROCHIMICA ACTA PART A MOLECULAR AND BIOMOLECULAR SPECTROSCOPY · SEPTEMBER 2013

Impact Factor: 2.35 · DOI: 10.1016/j.saa.2013.09.060 · Source: PubMed

1 AUTHOR:

Andrea Alparone
University of Catania
67 PUBLICATIONS **791** CITATIONS

SEE PROFILE

Spectrochimica Acta Part A: Molecular and Biomolecular Spectroscopy 117 (2014) 669–678

Contents lists available at ScienceDirect

Spectrochimica Acta Part A: Molecular and Biomolecular Spectroscopy

journal homepage: www.elsevier.com/locate/saa

Anharmonic IR and Raman spectra and electronic and vibrational (hyper)polarizabilities of barbituric, 2-thiobarbituric and 2-selenobarbituric acids

Andrea Alparone *

Department of Chemistry, University of Catania, viale A. Doria 6, Catania 95125, Italy

HIGHLIGHTS

- We computed IR and Raman spectra of barbituric, 2-thio and 2-selenobarbituric acids.
- Vibrational wavenumbers were obtained using harmonic and anharmonic PT2 treatment.
- We calculated electronic and vibrational (hyper)polarizabilities $\langle\alpha\rangle$ and $\langle\gamma\rangle$.
- Electronic absorption spectra were obtained using TD-DFT calculations.
- The γs of 2-selenobarbituric acid are 3–4 times larger than those of barbituric acid.

GRAPHICAL ABSTRACT

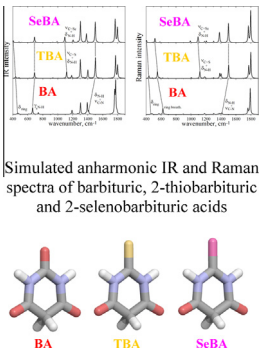

Simulated anharmonic IR and Raman spectra of barbituric, 2-thiobarbituric and 2-selenobarbituric acids

ARTICLE INFO

Article history:
Received 12 February 2013
Received in revised form 5 September 2013
Accepted 16 September 2013
Available online 25 September 2013

Keywords:
Barbituric acid
2-Thiobarbituric acid
2-Selenobarbituric acid
IR and Raman spectra
Anharmonic vibrational computations
(Hyper)polarizabilities

ABSTRACT

Infrared, Raman and electronic absorption spectra, electronic and vibrational (hyper)polarizabilities, of barbituric, 2-thiobarbituric and 2-selenobarbituric acids were studied in gas using *ab initio* and density functional theory levels. The vibrational spectra were computed using harmonic and anharmonic methods. Anharmonic contributions improve the agreement between calculated and available experimental wavenumbers, especially in the highest-energy spectral region (wavenumbers >1700 cm^{-1}). Vibrational and electronic transitions potentially useful to identify the investigated compounds were explored. The electronic and vibrational hyperpolarizabilities for the IDRI nonlinear optical (NLO) process at the λ value of 790 nm were computed. Supported by spectroscopic results, electronic and vibrational polarizabilities and second-order hyperpolarizabilities increase progressively in the order barbituric acid < 2-thiobarbituric acid < 2-selenobarbituric acid. The seleno-derivative is predicted to be ca. three/four times more hyperpolarizable than the barbituric acid. The Se → O or Se → S substitutions can be practical strategies to enhances the NLO properties of barbituric and thiobarbituric acid-based materials.

Introduction

Barbituric acid (**BA**) is the parent compound of barbiturates, an important class of pharmaceutically active substances [1–3]. Recently, **BA** derivatives have also received great attention for nanoscience applications [4,5]. Organic molecules based on **BA** or on its sulfur derivative (thiobarbituric acid) were proposed as promising nonlinear optical (NLO) materials [6–13]. 2-Thiobarbituric acid (**TBA**) is also employed as inhibitor of corrosion phenomena [14] and to check auto-oxidation mechanisms of fats and oils [15]. Experimental and theoretical investigations in vacuum, solution and solid phases unequivocally established that **BA** exist as a trike-to tautomeric form (Fig. 1) [16–24]. On the other hand, **TBA** can exist as 4,6-diketo-2-thione tautomer or in mixtures with enolic

* Tel.: +39 95 7385008.
E-mail address: agalparone@unict.it

1386-1425/$ - see front matter © 2013 Elsevier B.V. All rights reserved.
http://dx.doi.org/10.1016/j.saa.2013.09.060

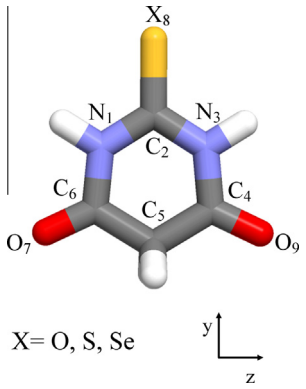

Fig. 1. Molecular structure of barbituric, 2-thiobarbituric and 2-selenobarbituric acids. White (hydrogen), gray (carbon), cyan (nitrogen), red (oxygen), yellow (X atom = oxygen, sulfur, selenium). (For interpretation of the references to color in this figure legend, the reader is referred to the web version of the article.)

forms, especially in condensed media [16–18,25]. Little is known about seleno-derivatives of barbituric acid [26,27]. Brunetti and Piacente [26], studying 2-selenobarbituric acid (**SeBA**) noted that its vapor pressures is lower than those of **BA** and **TBA**, being expected to be relatively more stable to heating and sublimation processes. The use of **SeBA** derivatives for NLO applications in alternative to **BA** and **TBA** moieties is rather intriguing, because atom substitution with a heavier one is a practical approach to enhance NLO properties [28–31]. A well-established example is given by the furan homologs: on passing from C_4H_4O to C_4H_4Se the second-order hyperpolarizability increases by about a factor of two [28,29].

In this work we extensively characterized the structure of the lowest-energy tautomer of **BA**, **TBA** and **SeBA** through vibrational and electronic spectra simulated by quantum mechanical methods. Specifically, the electronic spectra were computed using Time-dependent Density Functional Theory (TD-DFT), whereas IR and Raman spectra were obtained through harmonic and anharmonic calculations. As well-known, under harmonic approximation DFT methods systematically overestimate vibrational experimental wavenumbers. In order to correct experiment/calculation discrepancies three strategies are commonly adopted: (a) computing anharmonic corrections explicitly through second-order perturbation [32–36] or variational [37–41] techniques; (b) performing scaled force-field procedures [42]; and (c) using pre-calculated scaling factors [43]. In the present study we used the first approach, introducing anharmonic corrections through second-order perturbation theory (PT2) as described in details by Barone [32].

Additionally, we calculated and analyzed static and frequency-dependent electronic and vibrational polarizabilities and second-order hyperpolarizabilities, assisted by spectroscopic surveys. There are many examples in literature showing that the vibrational (hyper)polarizabilities are comparable to the electronic counterparts, giving important contributions to the total properties [30,31,44–50].

Computational details

All computations were carried out using Gaussian 03 [51] and Gamess packages [52]. The neutral ground-state geometries of **BA**, **TBA** and **SeBA** (Fig. 1) were fully optimized in vacuum using coupled-cluster with single and double excitations (CCSD) and B97-1 DFT [53] levels with Pople's 6-31G** and 6-31+G**, as well as Dunning's correlation-consistent aug-cc-pVDZ basis sets. The B97-1 functional was previously used with success for geometry optimization of cyclic compounds [54–57]. Vibrational wavenumbers were calculated under the harmonic approximation. In addition, we performed anharmonic computations using the PT2 procedure as implemented in Gaussian 03. The fundamental wavenumber values (ν_i) were obtained from the harmonic data (ω_i), diagonal (χ_{ii}) and off diagonal (χ_{ij}) anharmonic constants [32]:

$$\nu_i = \omega_i + 2\chi_{ii} + \frac{1}{2}\sum_{j\neq i}\chi_{ij} \tag{1}$$

The plots of simulated IR and Raman spectra were represented as pure Lorentzian line shapes with full widths at half maximum of 10 cm^{-1}, as frequently adopted in the literature [58–61].

For the investigated acids, we evaluated the static electronic polarizability α^e_{ii} ($i = x, y, z$), and second-order hyperpolarizability γ^e_{iijj} ($i, j = x, y, z$) components using Hartree–Fock (HF) and B97-1 levels with the aug-cc-pVDZ basis set. This basis set incorporates polarized and diffuse functions and is proven to give satisfactory performances for calculating response electric properties [56,57,62–65]. The importance of electron correlation effects and polarized and diffuse basis sets to accurately predict electronic (hyper)polarizabilities is widely recognized [66–69]. There are indications in literature showing that the B97-1 functional reproduces reasonably well response electric properties obtained using correlated *ab initio* methods [56,57,63,70]. However, electron correlation effects were here explored on **BA** as a test case, using the *ab initio* Møeller–Plesset second-order perturbation theory (MP2) with the aug-cc-pVDZ basis set. The HF/aug-cc-pVDZ α^e_{ii} and γ^e_{iijj} components were calculated analytically within the time dependent HF (TD-HF) theory [71]. The B97-1/aug-cc-pVDZ and MP2/aug-cc-pVDZ (hyper)polarizabilities were here obtained numerically through a finite field (FF) scheme previously described by Kurtz and co-workers [72], using an electric field strength amplitude of 0.005 a.u. The accuracy of the numerical procedure was verified at the HF level by comparing the FF-HF and TD-HF values. Additionally, we computed frequency-dependent electronic hyperpolarizabilities for the Intensity Dependent Refractive Index [IDRI, $\gamma^e(-\omega;\ \omega,\ \omega,\ -\omega)$] NLO phenomenon, using the TD-HF/aug-cc-pVDZ level at the characteristic wavelength (λ) of 790 nm ($\hbar\omega$ = 0.05767 a.u.) of the diode laser. Beside to the electronic (hyper)polarizabilities we also evaluated the vibrational counterparts [73]. The vibrational (hyper)polarizabilities (α^ν and γ^ν) were here determined at the HF/aug-cc-pVDZ level on the geometry optimized at the same level. It was previously demonstrated that, in comparison to electric response properties, electron correlation effects have a minor influence on the vibrational (hyper)polarizabilities [57,74].The $\alpha^\nu(0;\ 0)$ and $\gamma^\nu(-\omega;\ \omega,\ \omega,\ -\omega)$ values were obtained under the double harmonic oscillator treatment [73], and by invoking the infinite optical frequency approximation for $\gamma^\nu(-\omega;\ \omega,\ \omega,\ -\omega)$ [75]:

$$\alpha^\nu_{ij}(0;\ 0) = [\mu^2]^{0,0} = \sum_a^{3N-6}\frac{\left(\frac{\partial\mu^e_i}{\partial Q_a}\right)_0\left(\frac{\partial\mu^e_j}{\partial Q_a}\right)_0}{\omega_a^2} \tag{2}$$

$$\begin{aligned}\gamma^\nu_{ijkl}(-\omega;\omega,\omega,-\omega)_{\omega\to\infty} &= \frac{2}{3}[\alpha^2]^{0,0}\\ &= \frac{2}{3}\times\frac{1}{8}\sum P_{-\sigma,1,2,3}\\ &\quad\times\sum_a^{3N-6}\frac{\left(\frac{\partial\alpha^e_{ij}}{\partial Q_a}\right)_0\left(\frac{\partial\alpha^e_{kl}}{\partial Q_a}\right)_0}{\omega_a^2}\end{aligned} \tag{3}$$

where Q_a is the normal mode coordinate and ω_a is the vibrational wavenumber value.

In the present work we report α_{ii} and γ_{iijj} components, as well as the isotropically average invariants $\langle\alpha\rangle$ and $\langle\gamma\rangle$:

$$\langle\alpha\rangle = \frac{1}{3}\sum_i\alpha_{ii} \tag{4}$$

Table 1
Geometrical parameters of barbituric (**BA**), 2-thiobarbituric (**TBA**) and 2-selenobarbituric (**SeBA**) acids in gas phase.

Parameter [a]	**BA**					**TBA**				**SeBA**			
	CCSD/6-31G**	B97-1/6-31G**	B97-1/6-31+G**	B97-1/aug-cc-pVDZ	Exp.[b]	CCSD/6-31G**	B97-1/6-31G**	B97-1/6-31+G**	B97-1/aug-cc-pVDZ	CCSD/6-31G**	B97-1/6-31G**	B97-1/6-31+G**	B97-1/aug-cc-pVDZ
$r(N_1C_2)$	1.390	1.394	1.394	1.393	1.396	1.377	1.378	1.380	1.379	1.372	1.374	1.375	1.375
$r(N_3C_4)$	1.389	1.391	1.391	1.391	1.393	1.393	1.397	1.395	1.395	1.395	1.397	1.395	1.397
$r(C_4C_5)$	1.515	1.522	1.521	1.519	1.526	1.513	1.590	1.518	1.517	1.513	1.520	1.518	1.518
$r(C_2X_8)$	1.213	1.213	1.215	1.215	1.215	1.648	1.658	1.656	1.661	1.790	1.789	1.785	1.808
$r(C_4O_9)$	1.215	1.213	1.216	1.215	1.210	1.214	1.212	1.215	1.214	1.214	1.213	1.215	1.214
$r(N_1H)$	1.010	1.014	1.015	1.015	1.009	1.010	1.014	1.015	1.015	1.010	1.014	1.016	1.016
$r(C_5H)$	1.090	1.096	1.097	1.100	1.085	1.091	1.097	1.097	1.100	1.091	1.097	1.097	1.101
rms deviation	0.006	0.005	0.006	0.007									
$\angle(N_1C_2O_8)$	122.7	122.7	122.5	122.5	122.1	122.7	122.5	122.5	122.4	122.5	122.3	122.3	122.2
$\angle(N_1C_6O_7)$	121.4	121.4	121.3	121.1	121.0	120.9	120.9	120.8	120.7	120.9	121.0	120.8	120.7
$\angle(C_2N_1C_6)$	128.0	128.1	127.7	127.6	127.1	128.2	128.1	127.9	127.7	127.9	128.0	127.8	127.6
$\angle(N_1C_2N_3)$	114.6	114.6	115.0	115.1	115.7	114.5	115.0	115.0	115.3	115.1	115.3	115.4	115.5
$\angle(C_4C_5C_6)$	117.7	118.0	117.8	117.8	117.4	117.1	117.4	117.2	117.3	117.1	117.4	117.1	117.2
$\angle(HC_5C_4)$	108.1	108.1	108.2	108.2	108.0	108.2	108.3	108.3	108.3	108.2	108.3	108.3	108.3
$\angle(HC_5H)$	106.2	105.7	105.8	105.8		106.3	105.7	105.8	105.8	106.3	105.7	105.8	105.8
$\angle(N_1C_6C_5)$	115.9	115.6	115.9	115.9	116.4	116.0	115.9	116.1	116.0	115.9	115.6	116.0	116.0
$\angle(C_5C_6O_7)$	122.7	123.0	122.8	122.9	122.6	123.1	123.4	123.2	123.2	123.2	123.4	123.2	123.4
$\angle(C_6N_1H)$	116.7	116.8	117.0	117.1	116.9	115.8	116.1	116.2	116.5	116.1	116.2	116.2	116.4
rms deviation	0.6	0.7	0.4	0.4									

[a] Bond lengths in Å, angles in °. See Fig. 1 for atom numbering.
[b] Gas phase electron diffraction data taken from Ref. [24].

$$\langle\gamma\rangle = \frac{1}{15}\sum_{i,j}(\gamma_{iijj} + \gamma_{ijij} + \gamma_{ijji}) \quad (5)$$

where $i, j = x, y, z$.

The computed (hyper)polarizabilities are expressed in atomic units throughout the work. Conversion factor to the SI are: 1 a.u. of α $(e^2a_0^2E_h^{-1}) = 1.648778 \times 10^{-41}$ C^2 m^2 J^{-2}; 1 a.u. of γ $(e^4a_0^4E_h^{-3}) = 6.235377 \times 10^{-65}$ C^4 m^4 J^{-3}.

Results and discussion

Geometries

There are many theoretical studies in the literature about the relative stability of the tautomers of **BA** and **TBA** [16–21]. All computations undoubtedly establish that, in vacuum the triketo and 4,6-diketo-2-thione tautomers are the predominant forms of **BA** and **TBA**, respectively. The next most stable structure for **BA** and **TBA** is characterized by enolic and/or thio-enolic groups, lying ca. 10 kcal/mol above the most stable tautomer. Thus, these forms are expected to be a negligible fraction in the gas phase and are not considered in the subsequent part of the work.

The geometries of the most stable tautomer of **BA**, **TBA** and **SeBA** (Fig. 1) were investigated in details as a function of the level of theory and basis set. To this purpose we performed some calculations using the CCSD/6-31G**, B97-1/6-31G**, B97-1/6-31+G** and B97-1/aug-cc-pVDZ methods. The results are collected in Table 1 together with the experimental values recently obtained from electron diffraction measurements [24]. A normal mode analysis performed at the B97-1/6-31+G** level on **BA**, **TBA** and **SeBA**, yielded no imaginary wavenumbers, confirming that these forms correspond to equilibrium structures on the potential energy surfaces. On the whole the B97-1/6-31G** data agree with the CCSD/6-31G** computations, with deviation within 0.01 Å for bond lengths and 0.5° for bond angles. The basis set enlargement (6-31G** → 6-31+G**) provides quite negligible effects, the largest variations being within 0.004 Å for bond lengths and 0.5° for bond angles. The use of the Dunning's basis set does not produce relevant consequences on the structural data, except for the C=Se bond length which increases by 0.023 Å when passing from the B97-1/6-31+G** to B97-1/aug-cc-pVDZ level. In the case of the **BA**, we can compare our theoretical values with the experimental figures. As can be appreciated from the data reported in Table 1, the agreement is satisfactory at all the used levels, with root mean square deviations {rms $= \left[\frac{1}{n}\sum_i^n (x_i^{exp.} - x_i^{calc.})^2\right]^{1/2}$, where x_i is a geometrical parameter value} from experiment ranging from 0.005 Å to 0.007 Å for bond lengths and from 0.4° to 0.7° for bond angles.

IR and Raman spectra

In Tables 2–4 are listed the calculated harmonic and PT2 anharmonic wavenumbers, IR intensities (I_{IR}) and Raman activities (A_R) of **BA**, **TBA** and **SeBA** obtained in gas at the B97-1/6-31+G** level on the geometry optimized at the same level. These tables also include the available experimental fundamental frequencies for **BA** [76] and **TBA** [18]. Harmonic and anharmonic wavenumber values for overtones and combination bands were also computed and the results are collected in Tables S1–S6 of the Supplementary materials. The PT2 treatment in combination with DFT levels was previously employed with success, especially in the prediction of vibrational wavenumbers of cyclic compounds [54,55,77–82]. Experimentally, infrared spectra of **BA** and **TBA** were measured in Ar matrix by Barnes et al. [76] and by Ramondo et al. [18], respectively, which also provided assignments of some fundamentals. To the best of our knowledge, vibrational spectra of **SeBA** are lacking. On the theoretical side, the infrared spectra of **BA** and **TBA** were previously computed under the harmonic approximation at the MP2/6-311++G(d,p) and B3LYP/6-311++G(d,p) [18] levels. Neither experimental nor calculated Raman spectra are available in literature so far.

For every compound in total there are 33 vibrations, the anharmonic corrected wavenumber values being distributed in the range from 3451 to 78 cm^{-1}. The present assignments of the vibrational modes were based on the B97-1/6-31+G** computations and are in reasonable agreement with the experimental [18,76] and previous theoretical studies [18]. However, there are some severe

discrepancies between some theoretical (both harmonic and anharmonic) and experimental data as assigned by Ramondo et al. [18]. In particular, we note that, the present harmonic and anharmonic wavenumber values (Table 2) for mode nos. 10 and 13 of **BA** noticeably underestimate (by 50–120 cm^{-1}) the proposed observed figures at 1498 and 1353 cm^{-1}, respectively. Additionally, the experimental frequency of mode no. 9 of **TBA** at 1501 cm^{-1} is underestimated by both harmonic (−79 cm^{-1}) and anharmonic (−117 cm^{-1}) computations. Note that similar contradictions also occur between the experimental and harmonic B3LYP/6311++G(d,p) wavenumber values calculated by Ramondo et al. [18]. Therefore, it would be desirable to re-examine the experimental IR spectra of **BA** and **TBA**, which might involve the presence of other species. The results of Tables 2 and 3 show that, the B97-1/6-31+G** harmonic wavenumbers give rms deviations from experiment of 67 cm^{-1} for **BA** and 69 cm^{-1} for **TBA**, which reduce to 19 and 29 cm^{-1}, respectively, when anharmonic corrections are taken into account. In Fig. 2 we report the percentage deviation of the calculated wavenumbers from the available experimental data of **BA** and **TBA**. The better performances of the anharmonic computations are especially evident for the high-wavenumber stretching vibrations, reproducing the observed wavenumber values for the CH_2, N—H and C=O stretches within ~50 cm^{-1}. Note that for the harmonic approximation the corresponding deviations are somewhat larger, also reaching 200 cm^{-1}.

The lowest-energy IR and Raman regions (wavenumbers <400 cm^{-1}) show several weak peaks, not interesting enough to describe the investigated acids. Thus these spectral regions are not discussed in the present work. For all the investigated compounds, the highest-wavenumber infrared region is characterized by a relatively intense absorption (I_{IR} of ca. 110 km/mol) attributed to a pure asymmetric N—H bond stretching mode (ν_aN—H). Present anharmonic calculations locate this vibration at 3451, 3430 and 3425 cm^{-1} for **BA**, **TBA** and **SeBA**, respectively, to be compared with the observed data of 3437 cm^{-1} for **BA** and 3415 cm^{-1} for **TBA**. Interestingly, the anharmonic wavenumber ν_aN—H(**BA**) − ν_aN—H(**TBA**) difference of 21 cm^{-1} nicely reproduces the experimental datum of 22 cm^{-1} [18,76], which is underestimated by the harmonic approximation (−8 cm^{-1}). Fig. 3 displays the simulated anharmonic IR spectra of **BA**, **TBA** and **SeBA** in the 400–1900 cm^{-1} wavenumber range. At first sight one notices that **TBA** and **SeBA** show a similar spectral profile, somewhat different from **BA**. Not surprisingly, the IR spectra of **BA**, **TBA** and **SeBA** exhibit the most intense absorptions near 1750–1800 cm^{-1}, in correspondence of the C=O stretching (νC=O) transitions. The 1300–1500 cm^{-1} IR region is mainly characterized by three relatively intense peaks. As previously anticipated, **TBA** and **SeBA** present similar spectra with close wavenumbers and intensities, but different from the spectrum of **BA**. In facts, for **BA** the highest-energy absorption is placed at 1413 cm^{-1}, which is shifted downward by ca. 90 cm^{-1} with respect to **TBA** (and **SeBA**), in agreement with the observed spectra (80 cm^{-1}) [18,76]. In addition one notes that, when passing from **BA** to **TBA** (and **SeBA**) the I_{IR} value of this vibration increases by one order of magnitude. This transition is here assigned to in-plane N—H bending deformation (δN—H) with the contribution of νC—N motion (modes no. 8, 7 and 7 for **BA**, **TBA** and **SeBA**, respectively). A graphical representation of this mode is depicted in Fig. 4a. Near 1100 cm^{-1}, both the IR spectra of **TBA** and **SeBA** exhibit a visible peak, lacking for **BA**, which is placed at 1118 cm^{-1} (**TBA**) and 1094 cm^{-1} (**SeBA**). It is assigned to νC=S + δN—H [mode no. 15, Fig. 4b] and νC=Se + δN—H (mode no. 15) vibration, respectively. The corresponding absorption for **BA** (νC_2=O) is blue shifted by ca. 700 cm^{-1} with respect to **TBA** (mode no. 5, ν = 1791 cm^{-1}), in reasonable agreement with experiments (619 cm^{-1}). This result is consistent with the significantly different force constants, which at the B97-1/6-31+G** level are calculated to be 24.94 mdyne/Å for the νC_2=O vibration and 2.01 mdyne/Å for the νC=S + δN—H vibration.

The low-wavenumber spectral region is characterized by an isolated and moderately intense absorption (I_{IR} between 150 and 190 km/mol), here placed at 664, 690 and 690 cm^{-1} for **BA** (mode no. 21), **TBA** (mode no. 20) and **SeBA** (mode no. 20), respectively. This transition is attributed to a pure out-of-plane bending deformation of the N—H groups [γ_sN—H, Fig. 4c]. The corresponding experimental figures are 674 and 699 cm^{-1} for **BA** and **TBA**, respectively, the calculated anharmonic ν values being in error by −1.5% and −1.3%, respectively. At lower wavenumber values (400–500 cm^{-1}) there is a relatively less intense peak (I_{IR} between 40 and 50 km/mol), ascribed to in-plane ring bending deformation [δring, Fig. 4d] also involving the X_8 atom, with wavenumbers progressively decreasing in the order **BA** (464 cm^{-1}, mode no. 27) > **TBA** (438 cm^{-1}, mode no. 28) > **SeBA** (406 cm^{-1}, mode no. 28).

The calculated anharmonic Raman spectra of the investigated compounds between 400 and 1900 cm^{-1} are shown in Fig. 5. In the high-wavenumber spectral region the symmetrical N—H, CH_2 and C=O stretching modes are strong transitions for all the acids (with A_R values between 86 and 199 $Å^4$/amu). Similarly to the infrared results, the δNH + νC—N vibration for **TBA** and **SeBA** located near 1500 cm^{-1} (mode no. 7) presents a rather intense peak (with A_R values of ca. 50–60 $Å^4$/amu), whereas the corresponding peak for **BA** is one order of magnitude less intense and concomitantly shifted downward by ca. 90 cm^{-1}. Furthermore, the νC=X + δN—H (X = S, Se) transition for **TBA** and **SeBA** is also visible in the Raman spectra (A_R ca. 20 $Å^4$/amu) at ca. 1100 cm^{-1}. The corresponding peak for **BA** located at ν = 1791 cm^{-1}, is predicted to be ca. four times more active.

Near 1400 cm^{-1} **TBA** shows two equally intense Raman peaks, separated by 18 cm^{-1} (modes no. 8 and 9) and assigned to (1) νC—N + δN—H and (2) CH_2 scissoring vibrations. Differently, for **SeBA** the corresponding bands are merged to each other (modes no. 8 and 9, $\Delta\nu$ = 4 cm^{-1}). These results are consequence of a quite different anharmonic effect on these vibrations: in the case of **TBA**, the anharmonic correction increases the peak separation by 8 cm^{-1}, whereas for **SeBA** it decreases the separation by 15 cm^{-1}. Unfortunately experimental Raman spectra are unavailable to date. However by inspecting the experimental IR spectrum of 2-thiobarbituric acid [18], below 1400 cm^{-1} one notes the presence of a unassigned little intense band, which is sufficiently apart from the stronger peak located at 1416 cm^{-1} (mode no. 8). Thus this unassigned transition could correspond to mode no. 9, placed at 1384 cm^{-1} by the B97-1/6-31+G** anharmonic computations.

The low-energy spectral region of **BA** shows an active Raman peak at 625 cm^{-1} (mode no. 23, A_R = 20 $Å^4$/amu), here attributed to ring breathing deformation mode. The corresponding transition for **TBA** and **SeBA** exhibits similar Raman activities, but is located at lower wavenumber values, 552 cm^{-1} (mode no. 25) and 518 cm^{-1} (mode no. 25), respectively. A plot of this vibration is given in Fig. 4e.

In conclusion, the above IR and Raman spectra suggest that, the presence of a visible peak near 1100 cm^{-1} and/or near 1500 cm^{-1} could be potentially useful to detect **TBA** and/or **SeBA**, excluding the parent compound **BA**. On the other hand, **TBA**/**SeBA** identification can be a harder task, since the spectral differences are much less pronounced.

The present calculated I_{IR} and A_R values allow us to determine two interesting spectroscopic properties: the summation over IR intensities (ΣI_{IR}) and summation over Raman activities (ΣA_R). Generally, these parameters are specific of a given structure and were previously used to characterize series of homologs [83] and isomers [84,85]. Recently they have been also proposed as possible molecular descriptors [84,85]. Using the B97-1/6-31+G** data

Table 2
Calculated harmonic, ω and anharmonic, ν wavenumbers (cm^{-1}), IR intensities, I_{IR} (km/mol) and Raman activities A_R (amu/Å^4) of barbituric acid.[a]

No.	Description[c]	Calc.				Exp.[b]
		ω	ν	I_{IR}	A_R	ν
1	ν_sN—H	3620	3450	50.6	139.5	3431
2	ν_aN—H	3618	3451	111.8	27.8	3437
3	ν_aCH$_2$	3118	2955	2.2	58.3	
4	ν_sCH$_2$	3077	2921	2.6	122.2	
5	νC$_2$=O	1838	1791	61.5	86.7	1764
6	νC$_2$=O + νC$_4$=O + νC$_6$=O	1818	1773	881.3	5.5	1754
7	νC$_4$=O + νC$_6$=O	1803	1760	584.7	18.5	1747
8	δN—H + νC—N	1453	1413	77.6	5.3	1433
9	δN—H + νC—N	1425	1395	319.6	2.5	1418
10	σCH$_2$	1416	1376	31.3	3.5	
11	δN—H + νC—N	1399	1354	8.1	1.0	
12	νC—N + δN—H	1350	1304	318.8	3.4	1322
13	wCH$_2$	1303	1265	15.4	0.6	
14	νC—N + νC—C	1240	1190	113.1	0.4	1222
15	τCH$_2$	1208	1181	0.0	3.1	1192
16	νC—N + νC—C	1021	998	7.8	1.3	1010
17	ρCH$_2$	950	937	8.2	0.1	
18	νC—C + νC—N	917	900	1.6	0.5	939
19	νC—C + νC—N	913	896	0.0	1.2	913
20	γC$_2$=O	739	741	43.5	0.1	754
21	γ_sN—H	685	664	188.8	0.5	674
22	γ_aN—H	676	666	0	0.0	
23	Ring breathing	634	625	0.9	20.1	634
24	γC=O	618	613	7.9	0.1	619
25	γC$_4$=O + γC$_6$=O + γN—H	585	572	0.0	2.8	
26	δring	487	480	12.5	2.7	486
27	δring	480	464	39.6	2.3	464
28	τring + γC$_4$=O + γC$_6$=O	475	473	0.4	0.0	
29	δC=O	380	379	16.5	3.2	
30	δC=O	379	378	35.1	0.6	
31	τring	140	144	1.8	0.0	
32	τring	122	125	0.0	0.1	
33	τring	36	102	11.2	0.0	
	rms deviation	67	19			

[a] All calculations were carried out at the B97-1 level with 6-31+G** basis set.
[b] Ref. [76].
[c] ν = stretching, δ = in-plane bending, σ = scissoring, τ = torsion, γ = out-of-plane bending, w = wagging, ρ = rocking, s = symmetric, a = asymmetric.

Table 3
Calculated harmonic, ω and anharmonic, ν wavenumbers (cm^{-1}), IR intensities, I_{IR} (km/mol) and Raman activities A_R (amu/Å^4) of 2-thiobarbituric acid.[a]

No.	Description[c]	Calc.				Exp.[b]
		ω	ν	I_{IR}	A_R	ν
1	ν_sN—H	3614	3433	31.5	120.4	
2	ν_aN—H	3610	3430	111.6	3.5	3415
3	ν_aCH$_2$	3114	2951	2.3	75.5	
4	ν_sCH$_2$	3074	2919	2.4	173.1	
5	ν_sC=O	1823	1799	361.9	86.0	1750
6	ν_aC=O	1802	1771	628.6	41.6	1740
7	δN—H + νC—N	1546	1502	581.9	46.0	1513
8	δN—H + νC—N	1432	1402	229.6	14.4	1416
9	σCH$_2$	1422	1384	4.2	16.5	
10	νC—N + δN—H	1380	1345	15.4	0.1	
11	νC—N + νC—C + δN—H	1345	1302	528.2	2.2	1330
12	wCH$_2$	1305	1277	14.3	0.5	1335
13	νC—N + νC—C + wCH$_2$	1243	1185	80.0	4.5	1220
14	τCH$_2$	1206	1179	0.0	3.0	1190
15	νC=S + δN—H	1150	1118	187.9	23.3	1145
16	νC—N + νC=S	1023	1004	3.2	2.6	
17	ρCH$_2$	948	935	10.2	0.3	934
18	νC—C + νC—N	898	880	1.9	0.3	
19	νC—C + νC—N	885	869	1.6	0.1	
20	γ_sN—H	713	690	166.3	0.7	699
21	γ_aN—H	692	682	0.0	0.0	
22	γC=S	614	622	2.8	1.4	
23	γN—H + γC=O + τCH$_2$	590	578	0.0	2.5	
24	δC=O + δC=S	584	578	1.6	0.1	
25	Ring breathing	554	552	0.6	23.4	
26	δring	490	483	15.7	1.4	
27	ρCH$_2$	477	479	0.0	0.1	
28	δring	444	438	50.7	8.8	
29	δC=O	367	366	5.7	5.9	
30	δC=S	256	240	11.3	2.4	
31	τring	131	133	0.0	0.0	
32	τring	118	118	1.9	0.4	
33	τring	38	98	11.9	0.0	
	rms deviation	65	29			

[a] All calculations were carried out at the B97-1 level with 6-31+G** basis set.
[b] Ref. [18].
[c] ν = stretching, δ = in-plane bending, σ = scissoring, τ = torsion, γ = out-of-plane bending, w = wagging, ρ = rocking, s = symmetric, a = asymmetric.

reported in Tables 2–4, the ΣI_{IR} values are 2954.4, 3065.2 and 3104.5 km/mol for **BA**, **TBA** and **SeBA**, respectively. The corresponding ΣA_R values are 513.9, 661.0 and 734.3 Å^4/amu, respectively. Both the ΣI_{IR} and ΣA_R values steadily enhance as the size of the X_8 atom increases, the ΣA_R differences being much more substantial.

Electronic and vibrational (hyper)polarizabilities

Table 5 collects the static electronic polarizabilities of **BA**, **TBA** and **SeBA**. For all the compounds the largest polarizability component is α^e_{yy} (see Fig. 1 for the Cartesian coordinate system), which produces ca. 40–50% of the total polarizabilities ($\alpha^e_{xx} + \alpha^e_{yy} + \alpha^e_{zz}$). As expected, B97-1/aug-cc-pVDZ calculations give $\langle\alpha^e\rangle$ values higher than those obtained at the HF/aug-cc-pVDZ level (by 12–13%), in consistency with previous studies [56,57,63,70]. The introduction of electron correlation at the MP2/aug-cc-pVDZ level on **BA** as a test case gives a positive contribution on all the components, increasing the HF/aug-cc-pVDZ $\langle\alpha^e\rangle$ value by 7.90 a.u. (+12%). Interestingly, we note that the B97-1/aug-cc-pVDZ calculations nicely reproduce the MP2/aug-cc-pVDZ $\langle\alpha^e\rangle$(**BA**) datum within 0.41 a.u. (−0.6%). All the polarizability components raise progressively in the order **BA** < **TBA** < **SeBA**, in agreement with experimental [86] and calculated [87] polarizabilities of O, S and Se atoms. In particular on passing from **BA** to **TBA** the B97-1/aug-cc-pVDZ $\langle\alpha^e\rangle$ value increases by 26.75 a.u. (+37%), whereas when going from **TBA** to **SeBA** the $\langle\alpha^e\rangle$ datum enhances by 11.46 a.u. (+12%). A similar trend occurs also for the static vibrational polarizabilities (Table 6), the $\langle\alpha^v\rangle/\langle\alpha^e\rangle$ ratio being predicted to be close to unity for all the studied compounds. It is of interest noting that, the dominant vibrational contribution to the polarizability is given by the low-wavenuber ring torsion mode (70–80%). The above electronic polarizability increases can be explained through the perturbation theory, which using the sum-over-state expression, relates the polarizability components α^e_{ii} to the excitation energies (E^{ng}) and to the corresponding electronic transition moments along the i-direction from the ground (g) to the n excited states (M^{ng}_i) [88]:

$$\alpha^e_{ii} = 2\sum_n \frac{(M^{ng}_i)^2}{E^{ng}} \quad (6)$$

Thus, we computed vertical electronic transitions to singlet excited states by means of the TD-DFT procedure [89–91], using the B97-1 functional with the aug-cc-pVDZ basis set on the B97-1/aug-cc-pVDZ geometries of the ground states. The spectroscopic parameters for the lowest-energy dipole-allowed transition of **BA**, **TBA** and **SeBA** are given in Table 7. The simulated absorption spectra in the 180–360 nm region were represented in Fig. 6, using Gaussian line shapes with full widths at half maximum of 20 nm. For **BA** the spectrum is characterized by two merged absorption bands, the most intense being located at λ_{max} = 190 nm, in agreement with previous calculations obtained at ZINDO (191 nm) and TD-DFT (187 nm) levels [17]. This transition regards a π–π^*

Table 4
Calculated harmonic, ω and anharmonic, ν wavenumbers (cm^{-1}), IR intensities, I_{IR} (km/mol) and Raman activities A_R (amu/Å^4) of 2-selenobarbituric acid.[a]

No.	Description[b]	Calc.			
		ω	ν	I_{IR}	A_R
1	ν_sN—H	3612	3430	27.6	113.7
2	ν_aN—H	3608	3425	106.7	0.7
3	ν_aCH$_2$	3113	2948	2.3	82.6
4	ν_sCH$_2$	3073	2921	2.0	199.1
5	ν_sC=O	1822	1797	414.1	105.4
6	ν_aC=O	1802	1766	644.8	52.9
7	δN—H + νC—N	1542	1500	566.0	63.9
8	νC—N + δN—H	1441	1382	234.9	19.6
9	σCH$_2$	1422	1378	3.6	20.3
10	νC—N + δN—H	1382	1353	3.2	0.1
11	νC—N + νC—C + δN—H	1343	1303	587.5	3.7
12	wCH$_2$	1306	1271	13.8	0.5
13	νC—N + νC—C + wCH$_2$	1244	1205	70.1	5.0
14	τCH$_2$	1208	1180	0.0	3.0
15	νC=Se + δN—H	1120	1094	148.8	19.3
16	νC—N + νC=Se	1004	991	20.9	5.0
17	ρCH$_2$	954	933	9.3	0.3
18	νC—C + νC—N	894	877	2.4	0.1
19	νC—C + νC—N	863	849	1.0	0.0
20	γ_sN—H	746	690	149.5	0.5
21	γ_aN—H	718	684	0.0	0.0
22	γC=Se	674	642	5.3	0.6
23	γN—H + γC=O + τCH$_2$	600	585	0.0	2.4
24	δC=O + δC=Se	578	572	1.0	0.5
25	Ring breathing	529	518	6.9	13.9
26	δring	490	483	15.9	1.1
27	ρCH$_2$	482	480	0.0	0.1
28	δring	408	406	45.7	6.9
29	δC=O	304	308	0.3	12.1
30	δC=OδC=Se	200	196	6.7	1.0
31	τring	146	138	0.0	0.0
32	τring	144	136	2.2	0.0
33	τring	77	78	12.0	0.0

[a] All calculations were carried out at the B97-1 level with 6-31+G** basis set.
[b] ν = stretching, δ = in-plane bending, σ = scissoring, τ = torsion, γ = out-of-plane bending, w = wagging, ρ = rocking, s = symmetric, a = asymmetric.

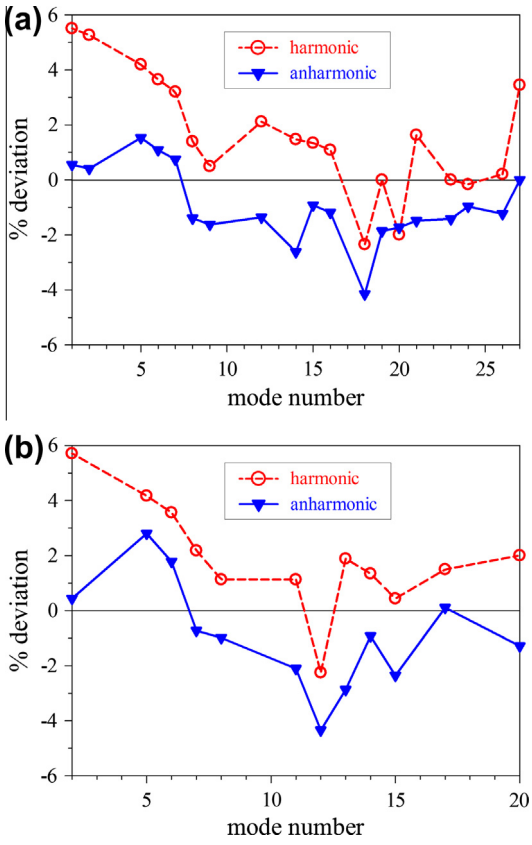

Fig. 2. Percentage errors relative to the experimental data [18,76] of the B97-1/6-31+G** vibrational wavenumbers of (a) barbituric acid and (b) 2-thiobarbituric acid. For the mode numbers see Tables 2 and 3.

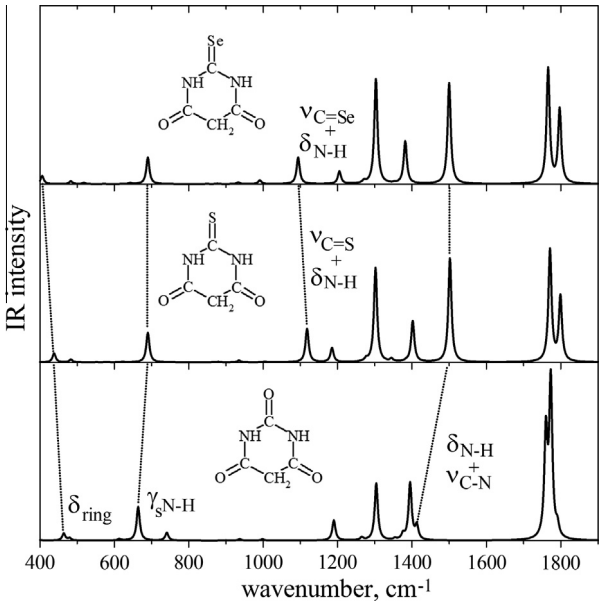

Fig. 3. Simulated anharmonic B97-1/6-31+G** IR spectra of barbituric, 2-thiobarbituric and 2-selenobarbituric acids.

HOMO-1 → LUMO excitation (Fig. 7). The corresponding λ_{max} values for **TBA** and **SeBA** are predicted at 265 nm and 299 nm, respectively. It is worth noting that, the B97-1/aug-cc-pVDZ λ_{max} data for **TBA** and **SeBA** agree satisfactorily with the experimental values of 265 and 298 nm obtained in phosphate–citrate buffer at pH = 7 [27], and with the λ_{max} = 264 nm for **TBA** measured in aqueous solution [17]. Additionally, our λ_{max}(**TBA**) value is in excellent agreement with the theoretical estimates of 265 and 266 nm previously determined by Zuccarello et al. [17], using TD-DFT and ZINDO computations, respectively. Following our TD-B97-1/aug-cc-pVDZ values, when passing from **BA** to **TBA** the absorption band is bathochromically shifted by 1.84 eV (75 nm), concomitantly increasing in intensity by ca. a factor of two. On the other hand, the spectral shift and intensity variation for the **TBA-SeBA** couple are sensibly smaller [E^{ng}(**SeBA**) − E^{ng}(**TBA**) = 0.54 eV; M_y^{eg}(**SeBA**) − M_y^{eg}(**TBA**) = 0.06 a.u.]. The present excitation energy data are consistent with the molecular orbital energies here computed at the B97-1/aug-cc-pVDZ level and shown in Fig. 7. On passing from **BA** to **TBA** (**SeBA**) the HOMO-1, which is localized on the C=O and C$_2$=X$_8$ groups, is destabilized by 1.33 eV (1.77 eV). By contrast the LUMO, mainly localized on the C$_2$=X$_8$ group, is stabilized by 0.78 eV (0.91 eV). As a consequences the HOMO-1 → LUMO energy gaps reduce with the size of the molecule, being predicted to be 6.97, 4.86 and 4.29 eV for **BA**, **TBA** and **SeBA**, respectively. These data are in reasonable agreement with the calculated E^{ng} values of 6.52, 4.68 and 4.14 eV, respectively. Thus, when the size of the X_8 atom increases, the E^{ng} value for the acid decreases and concomitantly the M_i^{ng} value raises, making foresee through Eq. (6) an increase of the polarizabilities. In the specific case, the HOMO-1 → LUMO electronic transition is mainly associated to the largest in-plane α_{yy}^e polarizability component. Indeed, using the expression (6) and invoking the two-state approximation restricted by HOMO-1 → LUMO excitation, we find a linear relationship between the B97-1/aug-cc-pVDZ α_{yy}^e values and the $(M_y^{ng})^2/E^{ng}$ ratios, with good statistics (the E^{ng} values were converted to a.u.):

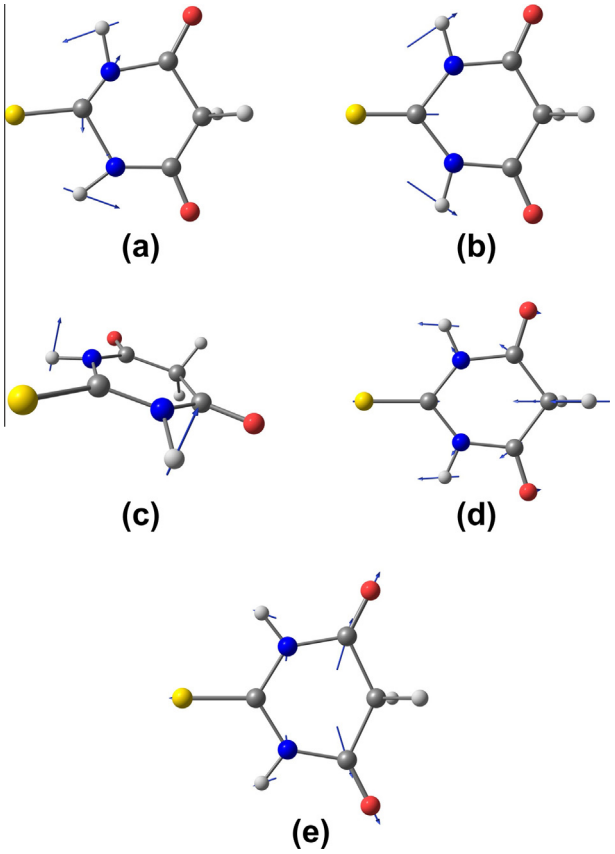

Fig. 4. Atomic vector displacements for normal modes of 2-thiobarbituric (See Table 3 for the mode numbering). (a) δN—H + νC—N (mode no. 7); (b) νC=S + δN—H (mode no. 15); (c) γ_sN—H (mode no. 20); (d) δring (mode no. 28); (e) ring breathing (mode no. 25).

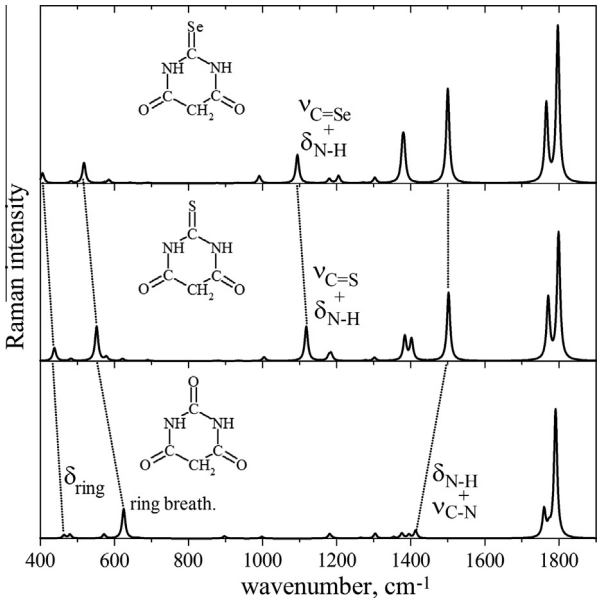

Fig. 5. Simulated anharmonic B97-1/6-31+G** Raman spectra of barbituric, 2-thiobarbituric and 2-selenobarbituric acids.

$$\alpha^e_{yy} = -32.06 + 0.52 \times [(M^{ng}_y)^2/E^{ng}] (r^2 = 0.99).$$

Furthermore, considering that Raman activities are derived by electronic polarizabilities [92], an excellent linear relationship between the present B97-1/6-31+G** ΣA_R values and the B97-1/aug-cc-pVDZ $\langle\alpha^e\rangle$ values was established:

$$\sum A_R = 98.95 + 5.71 \times < \alpha^e > (r^2 = 1.00).$$

Table 5 also includes the static electronic second-order hyperpolarizabilites for **BA**, **TBA** and **SeBA**. Similarly to the polarizabilities, the largest γ^e component is along the *y*-axis (γ^e_{yyyy}), giving ca. 30% of the total hyperpolarizabilities ($\gamma^e_{xxxx} + \gamma^e_{yyyy} + \gamma^e_{zzzz} + 2\gamma^e_{xxyy} + 2\gamma^e_{xxzz} + 2\gamma^e_{yyzz}$). As expected, the $\langle\gamma^e\rangle$ values increase when passing from the HF to the B97-1 functional by 50–90%. The introduction of electron correlation effects at MP2 level is positive. Indeed, when passing from HF/aug-cc-pVDZ to MP2/aug-cc-pVDZ level, the $\langle\gamma^e\rangle$ value of **BA** increases by 4582 a.u. (+88%). On the other hand, the B97-1/aug-cc-pVDZ $\langle\gamma^e\rangle$ (**BA**) value overestimates the MP2/aug-cc-pVDZ datum by 1384 a.u. (+16%). More importantly, all the components enhance steadily as the size of the X_8 atom increases, consistently

Table 5
Static electronic polarizabilities (a.u.) and second-order hyperpolarizabilities (a.u.) of barbituric (**BA**), 2-thiobarbituric (**TBA**) and 2-selenobarbituric (**SeBA**) acids.

	BA			**TBA**		**SeBA**	
	HF	B97-1	MP2	HF	B97-1	HF	B97-1
α^e_{xx}	41.48	43.70	44.30	54.50	56.12	60.96	62.60
α^e_{yy}	78.78	89.97	90.74	120.64	140.92	135.66	162.22
α^e_{zz}	74.60	83.64	83.52	90.53	100.07	97.69	107.14
$\langle\alpha^e\rangle$	64.95	72.44	72.85	88.55	99.19	98.10	110.65
γ^e_{xxxx}	2770	4123	3928	7995	9758	12,942	14,720
γ^e_{yyyy}	7974	14,779	12,162	23,234	35,050	36,485	45,008
γ^e_{zzzz}	5539	12,138	9468	13,918	24,541	21,185	34,624
γ^e_{xxyy}	1350	1920	2088	3448	6376	4403	8688
γ^e_{xxzz}	1041	1786	1739	2397	3645	3600	5056
γ^e_{yyzz}	2445	5206	4368	5720	11,158	6875	14,400
$\langle\gamma^e\rangle$	5191	9773	8389	13,655	22,341	20,074	30,128

All calculations were carried out with the aug-cc-pVDZ basis set on the B97-1/aug-cc-pVDZ geometry.

Table 6
Main vibrational contributions to the static vibrational polarizability of barbituric (**BA**), 2-thiobarbituric (**TBA**) and 2-selenobarbituric (**SeBA**) acids.

	ω (cm^{-1})	I_{IR} (km/mol)	Description[a]	$\langle\alpha^\nu\rangle$ (0; 0) (a.u.)[b]
BA	46	12.7	τring	53.81
	418	47.0	δC=O	2.41
	522	49.6	δring	1.63
	737	182.2	γC—H	3.01
	1962	1228.3	ν_sC=O	2.86
	1964	739.0	ν_{as}C=O	1.72
			Total	74.01 (64.95)[c]
TBA	44	13.5	τring	62.70
	477	90.0	δring	3.55
	779	174.4	γC—H	2.58
	1211	421.9	νC=S + δN—H	2.58
	1470	639.0	νC—N + νC—C + δN—H	2.65
	1690	827.5	δN—H + νC—N	2.60
			Total	86.15 (88.55)[c]
SeBA	39	13.9	τring	81.45
	119	3.1	τring	1.96
	441	80.2	δring	3.70
	789	154.9	γC—H	2.23
	1462	760.2	νC—N νC—C + δN—H	3.19
	1684	800.7	δN—H + νC—N	2.53
			Total	105.59 (98.10)[c]

Calculations were carried out at the HF/aug-cc-pVDZ level on the HF/aug-cc-pVDZ geometry.
[a] ν = stretching, δ = in-plane bending, γ = out-plane bending, τ = torsion, *s* = symmetric, as = asymmetric.
[b] The value in parentheses refers to the HF/aug-cc-pVDZ $\langle\alpha^e\rangle$ (0; 0) value.
[c] The $\frac{\langle\alpha^\nu\rangle(0;\,0)}{\langle\alpha^e\rangle(0;\,0)}$ ratios are 1.14, 0.97 and 1.08 for **BA**, **TBA** and **SeBA**, respectively.

Table 7
Vertical transition energy, E^{ng} (eV), wavelength, λ_{max} (nm), and dipole transition moment, M_y^{ng} (a.u.) of the lowest-allowed π–π^* singlet excited state of barbituric (**BA**), 2-thiobarbituric (**TBA**) and 2-selenobarbituric (**SeBA**) acids.

	BA	TBA	SeBA
E^{ng}	6.52	4.68	4.14
λ_{max}	190	265	299
M_y^{ng}	1.09	1.86	1.92
Description (coeff.)	H-1 → L (0.64); H-2 → L+1 (−0.18)	H-1 → L (0.62)	H-1 → L (0.61)

All calculations were carried out at the B97-1 level with the aug-cc-pVDZ basis set on the B97-1/aug-cc-pVDZ geometry.

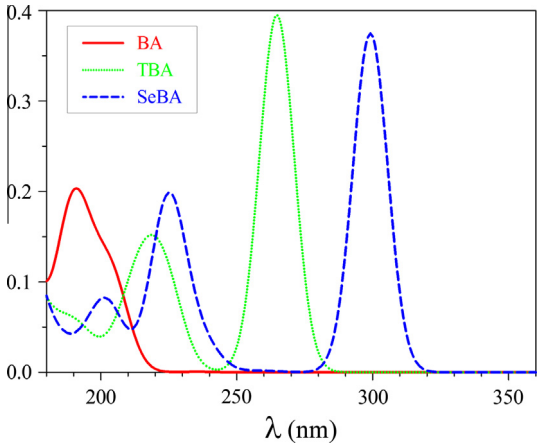

Fig. 6. Simulated B97-1/aug-cc-pVDZ electronic spectra of barbituric, 2-thiobarbituric and 2-selenobarbituric acids.

with theoretical atomic hyperpolarizability estimates ($\langle\gamma^e\rangle_O$ = 378 a.u., $\langle\gamma^e\rangle_S$ = 2979 a.u. and $\langle\gamma^e\rangle_{Se}$ = 7055 a.u. computed at the HF level) [29]. Specifically, with reference to the B97-1/aug-cc-pVDZ

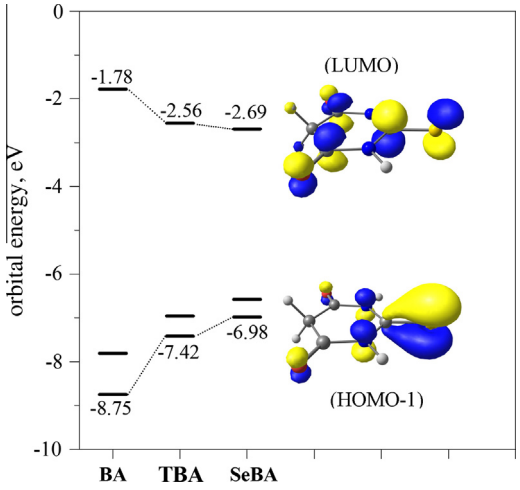

Fig. 7. Molecular orbital correlation diagram of barbituric, 2-thiobarbituric and 2-selenobarbituric acids. B97-1/aug-cc-pVDZ results.

data, when passing from **BA** to **TBA**, the $\langle\gamma^e\rangle$ value increases by 12,568 a.u. (+128%), whereas for the **TBA-SeBA** couple the difference is noticeably reduced (7787 a.u., +35%). The $\langle\gamma^e\rangle$(**SeBA**)/$\langle\gamma^e\rangle$(**BA**)) ratios are predicted to be 3.9 and 3.1 at the HF/aug-cc-pVDZ and B97-1/aug-cc-pVDZ levels, respectively. The $\langle\gamma^e\rangle$ variations among the title compounds are far superior to those obtained for the single atoms, denoting a some enhancing hyperpolarizability effect when increasing the size of the X_8 atom in the molecules. Finally, it is worth noting that present α^e_{yy} and $\langle\alpha^e\rangle$ values are linearly related to the corresponding γ^e_{yyyy} and $\langle\gamma^e\rangle$ data, with satisfactory statistics (α^e and γ^e values are expressed in a.u. and 10^3 a.u., respectively):

$$\gamma^e_{yyyy} = -22.72 + 0.41 \times \alpha^e_{yy} (r^2 = 1.00)$$

$$\langle\gamma^e\rangle = -28.33 + 0.52 \times \langle\alpha^e\rangle (r^2 = 0.99)$$

Table 8
Main vibrational contributions to the vibrational hyperpolarizability of barbituric (**BA**), 2-thiobarbituric (**TBA**) and 2-selenobarbituric (**SeBA**) acids.

	ω (cm^{-1})	A_{Raman} (Å^4/amu)	Description[a]	$\langle\gamma^v\rangle$ $(-\omega;\ \omega,\ \omega,\ -\omega)$ (a.u.)[b]
BA	418	2	δC=O	40
	522	1	δring	107
	687	16	ring breathing	488
	1992	50	ν_sC=O	175
	3230	111	ν_sCH$_2$	152
	3834	104	ν_sN—H	96
			Total	1352 (5825) [c]
TBA	402	3	δC=O	188
	477	4	δring	232
	599	18	Ring breathing	699
	1988	64	ν_sC=O	325
	3228	135	ν_sCH$_2$	273
	3831	80	ν_sN—H	110
			Total	2384 (17,427) [c]
SeBA	314	4	δring	522
	441	3	δC=O	215
	572	10	Ring breathing	427
	1993	86	ν_sC=O	282
	3228	144	ν_sCH$_2$	194
	3827	73	ν_sN—H	66
			Total	2561 (27,849) [c]

Calculations were carried out at the HF/aug-cc-pVDZ level on the HF/aug-cc-pVDZ geometry.
[a] ν = stretching, δ = in-plane bending, s = symmetric.
[b] The value in parentheses refers to the HF/aug-cc-pVD $\langle\gamma^e\rangle$ $(-\omega;\ \omega,\ \omega,\ -\omega)$ (0; 0)value at $\hbar\omega$ = 0.05767 a.u.
[c] The $\frac{\langle\gamma^v\rangle(-\omega;\omega,\omega,-\omega)}{\langle\gamma^e\rangle(-\omega;\omega,\omega,-\omega)}$ ratios are 0.23, 0.14 and 0.09 for **BA**, **TBA** and **SeBA**, respectively.

Similar γ^e vs. α^e relationships have been recently established for the series of the aliphatic amino acids [93,94] and oligoglycine chains [95].

As should be expected, the dispersion effects on the $\langle\gamma^e\rangle(-\omega;\ \omega,\ \omega,\ -\omega)$ values here determined at the $\hbar\omega = 0.05767$ a.u. are positive, increasing the static $\langle\gamma^e\rangle(0;\ 0,\ 0,\ 0)$ data by 634 a.u. (+12%), 3772 a.u. (+28%) and 7775 a.u. (39%) for **BA**, **TBA** and **SeBA**, respectively. Note that the largest percentage dispersion is found for the latter compound, in some consistency with the lowest E^{ng} value in the series of investigated acids (Table 7), even if other excited states through the summation-over-state expression [88] are expected to contribute to the second-order hyperpolarizabilities.

Table 8 collects the vibrational second-order hyperpolarizabilities computed in vacuum at the HF/aug-cc-pVDZ//HF/aug-cc-pVDZ level. The results show that, the order of the $\langle\gamma^v\rangle(-\omega;\ \omega,\ \omega,\ -\omega)$ values is analog to that obtained for the electronic counterparts. The $\langle\gamma^v\rangle(-\omega;\omega,\omega,-\omega)$ value for **SeBA** is greater than those for **BA** and **TBA** by 1209 a.u. (+89%) and 177 a.u. (+7%), respectively. For the NLO IDRI process, the vibrational hyperpolarizabilities are a non-negligible fraction of the total γ values, the $\langle\gamma^v\rangle(-\omega;\ \omega,\ \omega,\ -\omega)/\langle\gamma^e\rangle(-\omega;\ \omega,\ \omega,\ -\omega)$ ratios at $\hbar\omega = 0.05767$ a.u. being 0.23, 0.14 and 0.09 for **BA**, **TBA** and **SeBA**, respectively. Table 8 also includes the most contributing vibrational modes to the γ^v values. As can be seen from the data reported in the table, for **BA** and **TBA** the most important contribution involves the ring breathing deformation mode (see Fig. 4e), producing for both compounds ca. 1/3 of the total $\langle\gamma^v\rangle(-\omega;\ \omega,\ \omega,\ -\omega)$ value. At the HF/aug-cc-pVDZ level, in qualitative agreement with the B97-1/6-31+G** data (Tables 2–4), the ring breathing deformation is characterized by a moderate Raman activity (16, 18 and 10 Å^4/amu for **BA**, **TBA** and **SeBA**, respectively) and is located at rather low-wavenumber values (at 687, 599 and 572 cm^{-1} for **BA**, **TBA** and **SeBA**, respectively). For **SeBA**, beside to the ring breathing vibration, another relevant contribution to γ^v is given by the δring mode placed at 314 cm^{-1}. These vibrations together furnish ca. 37% of the total $\langle\gamma^v\rangle(-\omega;\ \omega,\ \omega,\ -\omega)$ value for **SeBA**.

Conclusions

In this work we determined the geometries, vibrational and electronic spectra, static and dynamic electronic and vibrational (hyper)polarizabilities of the most stable tautomer of the series of **BA**, **TBA** and **SeBA**. The physicochemical properties were calculated in gas phase using HF, MP2, CCSD and B97-1 DFT levels with the 6-31G**, 6-31+G** and aug-cc-pVDZ basis sets.

The anharmonic corrections on the vibrational frequencies estimated by the PT2 approximation improve significantly the agreement between calculations and experiments, especially for the high-energy stretching vibrations. Both the IR and Raman spectra are potentially useful to discriminate **BA** from the sulfur and seleno derivatives. In particular, the spectral regions involving the relatively intense νC═X + δN—H (X = S, Se) and δN—H + νC—N transitions located near 1100 cm^{-1} and 1500 cm^{-1}, respectively, seem to be the most suitable. On the other hand, vibrational spectra are much less helpful to distinguish **TBA** from **SeBA**.

The electronic (hyper)polarizabilities steadily enhance as the size of the X_8 atom increases, the calculated $\langle\gamma^e\rangle$ values for the **BA** being smaller than the corresponding data for the seleno-derivative by a factor of three/four. The different electronic (hyper)polarizabilities among the investigated acids were elucidated through the perturbation theory within the two-state approximation, using electronic absorption spectral data. The vibrational second-order hyperpolarizabilites, similarly to the γ^e values, increase progressively as the size of the X_8 atom raises, furnishing a non-negligible contribution to the total γ value. By contrast, the γ^v/γ^e ratios increases in opposite direction. The results suggest that, **SeBA** moieties could be considered promising candidates in design of novel NLO materials in alternative to the widely used **BA** and **TBA** ones.

Appendix A. Supplementary material

Supplementary data associated with this article can be found, in the online version, at http://dx.doi.org/10.1016/j.saa.2013.09.060.

References

[1] J.T. Bojarski, J.L. Mokrosz, H.J. Bartoń, M.H. Paluchowska, Adv. Heterocycl. Chem. 38 (1985) 229–297.
[2] M. Willow, G.A.R. Johnston, Int. Rev. Neurobiol. 24 (1983) 15–49.
[3] B.A. Diwan, R.W. Nims, J.R. Henneman, J.M. Ward, R.A. Lubet, J.M. Rice, Arch. Toxicol. 66 (1992) 413–422.
[4] D.M. Bassani, Chimia 60 (2006) 175–178.
[5] A. Ikeda, Y. Tanaka, K. Nobusawa, J.-I. Kikuchi, Langmuir 23 (2007) 10913–10915.
[6] K. Kondo, S. Ochiai, K. Takemoto, M. Irie, Appl. Phys. Lett. 56 (1990) 718.
[7] K. Kondo, M. Fukutome, N. Ohnishi, H. Aso, Y. Kitaoka, T. Sasaki, Jpn. J. Appl. Phys. 30 (1991) 3419–3420.
[8] S.R. Marder, L.-T. Cheng, B.G. Tiemann, A.C. Friedli, M. Blanchard-Desce, J.W. Perry, J. Skindhøj, Science 263 (1994) 511–514.
[9] B.R. Cho, J.T. Je, S.J. Lee, S.H. Lee, H.S. Kim, S.J. Jeon, O.-K. Song, C.H. Wang, J. Chem, Soc, Perkin Trans. 2 (1996) 2141–2144.
[10] D. Lu, B. Marten, Y. Cao, M.N. Ringnalda, R.A. Friesner, W.A. Goddard III, Chem. Phys. Lett. 242 (1995) 543–547.
[11] J. Garín, J. Orduna, J.I. Rupérez, R. Alcalá, B. Villacampa, C. Sánchez, N. Martín, J.L. Segura, M. González, Tetrahedron Lett. 39 (1998) 3577–3580.
[12] C.-C. Hsu, S. Liu, C.C. Wang, C.H. Wang, J. Chem. Phys. 114 (2001) 7103–7108.
[13] B.B. Ivanova, M. Spiteller, Cryst. Growth Des. 10 (2010) 2470–2474.
[14] M. Ozcan, R. Solmaz, G. Kardas, I. Dehri, Colloids Surf. A 325 (2008) 57–63.
[15] M. Guzmán-Chozas, I.M. Vicario-Romero, R. Guillén-Sans, J. Am. Oil Chem. Soc. 75 (1998) 1711–1715 (and references therein).
[16] S. Millefiori, A Millefiori, J. Heterocyclic Chem. 26 (1989) 639–644.
[17] F. Zuccarello, G. Buemi, C. Gandolfo, A. Contino, Spectrochim. Acta A 59 (2003) 139–151.
[18] F. Ramondo, A. Pieretti, L. Gontrani, L. Bencivenni, Chem. Phys. 271 (2001) 293–308.
[19] K. Senthilkumar, P. Kolandaivel, J. Comput. Aided Mol. Des. 16 (2002) 263–272.
[20] S. Ralhan, N.K. Ray, J. Mol. Struct. (Theochem) 634 (2003) 83–88.
[21] R. Kakkar, V. Katoch, J. Mol. Struct. (Theochem) 578 (2002) 169–175.
[22] G.A. Jeffrey, S. Ghose, J.O. Warwicker, Acta Crystallogr. 14 (1961) 881–887.
[23] W. Bolton, Acta Crystallogr. 16 (1963) 166–173.
[24] O.V. Dorofeeva, I.I. Marochkin, N.M. Karasev, I.F. Shishkov, H. Oberhammer, Struct. Chem. 22 (2011) 419–425.
[25] M.V. Roux, R. Notario, D.H. Zaitsau, V.N. Emel'yanenko, S.P. Verevkin, J. Phys. Chem. A 116 (2012) 4639–4645 (and references therein).
[26] B. Brunetti, V. Piacente, J. Chem. Eng. Data 44 (1999) 809–812.
[27] H.G. Mautner, E.M. Clayton, J. Am. Chem. Soc. 23 (1959) 6270–6273.
[28] K. Kamada, M. Ueda, H. Nagao, K. Tawa, T. Sugino, Y. Shimizu, K. Ohta, J. Phys. Chem. A 104 (2000) 4723–4734 (and references therein).
[29] S. Millefiori, A. Alparone, Chem. Phys. Lett. 332 (2000) 175–180.
[30] A. Alparone, A. Millefiori, S. Millefiori, Chem. Phys. 298 (2004) 75–86.
[31] A. Alparone, H. Reis, M.G. Papadopoulos, J. Phys. Chem. A 110 (2006) 5909–5918.
[32] V. Barone, J. Chem. Phys. 122 (2005). pp. 014108/1–10.
[33] D.A. Clabo, W.D. Allen, R.B. Remington, Y. Yamaguchi, H.F. Schaefer III, Chem. Phys. 123 (1988) 187–239.
[34] W. Schneider, W. Thiel, Chem. Phys. Lett. 157 (1989) 367–373.
[35] J. Neugebauer, B.A. Hess, J. Chem. Phys. 118 (2003) 7215–7225.
[36] A.G. Csaszar, I.M. Mills, Spectrochim. Acta A 53 (1997) 1101–1122.
[37] J.M. Bowman, J. Chem. Phys. 68 (1978) 608–610.
[38] J.M. Bowman, Acc. Chem. Res. 19 (1986) 202–208.
[39] R.B. Gerber, M.A. Ratner, Adv. Chem. Phys. 70 (1988) 97–132.
[40] S. Carter, J.M. Bowman, L.B. Harding, Spectrochim. Acta A 53 (1997) 1179–1188.
[41] S. Carter, S. Culik, S. Carter, J.M. Bowman, N.C. Handy, Theor. Chem. Acc. 100 (1998) 191–198.
[42] P. Pulay, G. Fogarasi, G. Pongor, J.E. Boggs, A. Vargha, J. Am. Chem. Soc. 105 (1983) 7037–7047.
[43] G. Rauhut, P. Pulay, J. Phys. Chem. 99 (1995) 3093–3100.
[44] B. Champagne, Chem. Phys. Lett. 261 (1996) 57–65.
[45] O. Loboda, R. Zalesny, A. Avramopoulos, J.-M. Luis, B. Kirtman, N. Tagmatarchis, H. Reis, M.G. Papadopoulos, J. Phys. Chem. A 113 (2009) 1159–1170.
[46] E.A. Perpète, B. Champagne, B. Kirtman, J. Chem. Phys. 107 (1997) 2463–2480.
[47] A. Alparone, S. Millefiori, Chem. Phys. Lett. 416 (2005) 282–288.
[48] V. Librando, A. Alparone, Z. Minniti, J. Mol. Struct. (Theochem) 856 (2008) 105–111.

[49] H. Reis, M.G. Papadopoulos, A. Avramopoulos, J. Phys. Chem. A 107 (2003) 3907–3917.
[50] V.E. Ingamells, M.G. Papadopoulos, S.G. Raptis, Chem. Phys. Lett. 307 (1999) 484–492.
[51] M.J. Frisch, G.W. Trucks, H.B. Schlegel, G.E. Scuseria, M.A. Robb, J.R. Cheeseman, J.A. Montgomery Jr., T. Vreven, K.N. Kudin, J.C. Burant, J.M. Millam, S.S. Iyengar, J. Tomasi, V. Barone, B. Mennucci, M. Cossi, G. Scalmani, N. Rega, G.A. Petersson, H. Nakatsuji, M. Hada, M. Ehara, K. Toyota, R. Fukuda, J. Hasegawa, M. Ishida, T. Nakajima, Y. Honda, O. Kitao, H. Nakai, M. Klene, X. Li, J.E. Knox, H.P. Hratchian, J.B. Cross, V. Bakken, C. Adamo, J. Jaramillo, R. Gomperts, R.E. Stratmann, O. Yazyev, A.J. Austin, R. Cammi, C. Pomelli, J.W. Ochterski, P.Y. Ayala, K. Morokuma, G.A. Voth, P. Salvador, J.J. Dannenberg, V.G. Zakrzewski, S. Dapprich, A.D. Daniels, M.C. Strain, O. Farkas, D.K. Malick, A.D. Rabuck, K. Raghavachari, J.B. Foresman, J.V. Ortiz, Q. Cui, A.G. Baboul, S. Clifford, J. Cioslowski, B.B. Stefanov, G. Liu, A. Liashenko, P. Piskorz, I. Komaromi, R.L. Martin, D.J. Fox, T. Keith, M.A. Al-Laham, C.Y. Peng, A. Nanayakkara, M. Challacombe, P.M.W. Gill, B. Johnson, W. Chen, M.W. Wong, C. Gonzalez, GAUSSIAN 03 Revision E0.1 Gaussian, J.A. Pople, Inc., Wallingford, CT, 2004.
[52] M.W. Schmidt, K.K. Baldridge, J.A. Boatz, S.T. Elbert, M.S. Gordon, J.H. Jensen, S. Koseki, N. Matsunaga, K.A. Nguyen, S.J. Su, T.L. Windus, M. Dupuis, J.A. Montgomery, J. Comput. Chem. 14 (1993) 1347–1363.
[53] F.A. Hamprecht, A.J. Cohen, D.J. Tozer, N.C. Handy, J. Chem. Phys. 109 (1998) 6264–6271.
[54] R. Burcl, N.C. Handy, S. Carter, Spectrochim. Acta A 59 (2003) 1881–1893.
[55] A. Alparone, Chem. Phys. 327 (2006) 127–136.
[56] A. Alparone, A. Millefiori, S. Millefiori, Chem. Phys. 312 (2005) 261–274.
[57] S. Millefiori, A. Alparone, Chem. Phys. 303 (2004) 27–36.
[58] V. Krishnakumar, S. Muthunatesan, Spectrochim. Acta A 61 (2005) 199–204.
[59] V. Krishnakumar, R.J. Xavier, Spectrochim. Acta A 61 (2005) 253–260.
[60] C.D. Keefe, J.E. Pickup, Spectrochim. Acta A 72 (2009) 947–953.
[61] V. Krishnakumar, R.J. Xavier, Spectrochim. Acta A 61 (2005) 1799–1809.
[62] A. Alparone, Theor. Chem. Acc. 131 (2012). pp. 1239/1–14.
[63] A. Alparone, Chem. Phys. 410 (2013) 90–98.
[64] T.P. Haley, E.R. Graybill, S.M. Cybulski, J. Chem. Phys. 124 (2006). pp. 204301/1–7.
[65] S. Millefiori, A. Alparone, Phys. Chem. Chem. Phys. 2 (2000) 2495–2501.
[66] G. Maroulis, A.J. Thakkar, J. Chem. Phys. 90 (1989) 366–370.
[67] E.F. Archibong, A.J. Thakkar, Chem. Phys. Lett. 201 (1993) 485–492.
[68] J.E. Rice, R.D. Amos, S.M. Colwell, N.C. Handy, J. Sanz, J. Chem. Phys. 93 (1990) 8828–8839.
[69] E.F. Archibong, A.J. Thakkar, Chem. Phys. Lett. 173 (1990) 579–584.
[70] S. Millefiori, A. Alparone, A. Millefiori, A. Vanella, Biophys. Chem. 132 (2008) 139–147.
[71] S.P. Karna, M. Dupuis, J. Comput. Chem. 12 (1991) 487–504.
[72] H.A. Kurtz, J.J.P. Stewart, K.M. Dieter, J. Comput. Chem. 11 (1990) 82–87.
[73] D.M. Bishop, Adv. Chem. Phys. 104 (1998) 1–40 (and references therein).
[74] O. Quinet, B. Champagne, J. Chem. Phys. 109 (1998) 10594–10602.
[75] D.M. Bishop, M. Hasan, B. Kirtman, J. Chem. Phys. 103 (1995) 4157–4159.
[76] A.J. Barnes, M.A. Stuckey, W.J. Orville-Thomas, L. Le Gall, J. Lauransan, J. Mol. Struct. 56 (1979) 15–27.
[77] C. Meganathan, S. Sebastian, I. Sivanesan, K.W. Lee, B.R. Jeong, H. Oturak, S. Sudha, N. Sundaraganesan, Spectrochim. Acta A 95 (2012) 331–340.
[78] E. Kavitha, N. Sundaraganesan, S. Sebastian, M. Kurt, Spectrochim. Acta A 77 (2010) 612–619.
[79] V. Librando, A. Alparone, Z. Minniti, J. Mol. Struct. (Theochem) 847 (2007) 23–24.
[80] U. Rani, H. Oturak, S. Sudha, N. Sundaraganesan, Spectrochim. Acta A 78 (2011) 1467–1475.
[81] J. Karpagam, N. Sundaraganesan, S. Kalaichelvan, S. Sebastian, Spectrochim. Acta A 76 (2010) 502–512.
[82] N.C. Handy, A. Willetts, Spectrochim. Acta A 53 (1997) 1169–1177.
[83] A. Alparone, A. Millefiori, S. Millefiori, J. Mol. Struct. (Theochem) 640 (2003) 123–131.
[84] A. Alparone, V. Librando, Struct. Chem. 23 (2012) 1467–1474.
[85] A. Alparone, V. Librando, Chemosphere 90 (2013) 158–163.
[86] T.M. Miller, CRC Handbook of Chemistry and Physics, 77th ed., CRC Press, Boca Raton, FL, 1996–1997.
[87] S. Millefiori, A. Alparone, J. Mol. Struct. (Theochem) 431 (1998) 59–78.
[88] B.J. Orr, J.F. Ward, Mol. Phys. 20 (1971) 513–526.
[89] R. Bauernschmitt, R. Ahlrichs, Chem. Phys. Lett. 256 (1996) 454–464.
[90] M.E. Casida, C. Jamorski, K.C. Casida, D.R. Salahub, J. Chem. Phys. 108 (1998) 4439–4449.
[91] R.E. Stratmann, G.E. Scuseria, M.J. Frisch, J. Chem. Phys. 109 (1998) 8218–8224.
[92] E.B. Wilson Jr., J.C. Decius, P.C. Cross, Molecular Vibrations: The Theory of Infrared and Raman Vibrational Spectra, Dover, New York, 1980.
[93] A. Alparone, Comput, Theor. Chem. 976 (2011) 188–190.
[94] A. Alparone, Comput. Theor. Chem. 980 (2012) 144.
[95] A. Alparone, Chem. Phys. Lett. 563 (2013) 88–92.